Journal of Nuclear Materials 393 (2009) 212–223

Contents lists available at ScienceDirect

Journal of Nuclear Materials

journal homepage: www.elsevier.com/locate/jnucmat

SIMS analysis of an UO_2 fuel irradiated at low temperature to 65 MWd/kgHM

C.T. Walker [a,*], S. Bremier [a], S. Portier [b], R. Hasnaoui [a], W. Goll [c]

[a] European Commission, Joint Research Centre, Institute for Transuranium Elements, P.O. Box 2340, D-76125 Karlsruhe, Germany
[b] Paul Scherrer Institut, CH-5232 Villigen PSI, Switzerland
[c] AREVA-NP GmbH, Freyeslebenstrasse 1, DE-91058 Erlangen, Germany

ARTICLE INFO

Article history:
Received 23 December 2008
Accepted 8 June 2009

ABSTRACT

The results of a wide-ranging post-irradiation study of a PWR nuclear fuel by secondary ion mass spectrometry are presented. The average cross-section burn-up and the radial burn-up profile were determined from the radial distributions of one or more of the stable isotopes of fission product Nd. The fission gas Kr was analysed in-situ in a nuclear fuel for the first time and an investigation of the total fission gas content of the high burn-up structure using depth profiling was performed. It was confirmed that Kr is together with Xe in the pores of the high burn-up structure, and that almost all the fission gas lost from the fuel matrix is contained in the pores. In addition to Xe and Kr, the volatile fission products Te, Cs, I and Rb were also detected in the pores. The radial distributions of the minor actinides in the fuel are also reported. It was found that ^{237}Np, unlike the isotopes of Pu, Am, and Cm, does not increase in concentration at the fuel rim.

1. Introduction

Since the 1960s electron probe microanalysis (EPMA) has been used to study the chemical behaviour of fission products in nuclear fuel. EPMA has supplied data on the radial distribution of retained xenon that has helped elucidate mechanisms involved in thermal fission gas release (see e.g. Ref. [1]). EPMA of the radial distribution of neodymium has revealed that the local burn-up of PWR fuel may be a factor of two or higher at the fuel surface due to enhanced production of ^{239}Pu by neutron capture [2]. EPMA has also played an important role in the investigation of the high burn-up structure (HBS) in the outer region of UO_2 fuel. The formation of the HBS is accompanied by a marked loss of xenon from the UO_2 grains [3]. Hence, by measuring the concentration of xenon in the outer region of the fuel it has been possible to follow the expansion of the HBS across the fuel section with increase in burn-up [4] and assign a burn-up threshold and temperature limit for the formation of the HBS [5]. It has become increasingly evident in recent years, however, that EPMA cannot deliver all the analytical data demanded by today's nuclear fuel performance research programmes. From the perspective of the investigation of irradiated nuclear fuel the main drawback of EPMA is that it does not measure isotopes. Another shortcoming is the detection limit, which for a radioactive sample is at best 200 ppm [6]. Mainly because of this it is not possible to obtain useful information on the behaviour of iodine and other low yield fission products. In addition, the fission gas krypton cannot be measured by EPMA. This is because co-incidence exists between the Kr Lα_1 X-ray line and the second order U Mα_1, and the Kr K X-ray lines have high critical excitation energy of 14.3 keV. A further major failing is that the fission gases trapped in pores and bubbles larger than about 0.1 μm are not detected [7,8]. Consequently, it has not been possible to deduce from EPMA of the HBS, whether the fission gas lost from the fuel grains is retained in the facetted pores that are a characteristic of the structure [9]. This has consequences for fuel safety studies, since it is not known with certainty how the HBS will respond to a reactivity insertion accident (RIA) [10]. For these reasons, secondary ion mass spectrometry (SIMS) of irradiated nuclear fuel has recently been introduced at the Institute for Transuranium Elements (ITU). Applying SIMS, the radial distribution of the fission product and actinide isotopes in nuclear fuel can be determined. Moreover, since the detection limit is of the order of 0.001 ppm the behaviour of important low yield fission products can be detected as can the fission gas contained in bubbles and pores, independent of their size. The main disadvantage of SIMS compared with EPMA is that the acquisition of quantitative data is not straightforward. Calibration curves, information about the local burn-up or EPMA element data must be employed in most cases to derive the isotope concentration.

This article reports the results of the first SIMS analysis of an irradiated UO_2 fuel sample carried out at ITU. The fuel had been irradiated at low temperature to a burn-up of 65 MWd/kgHM in a commercial PWR. The sample was chosen because an earlier EPMA investigation had revealed no migration or release of caesium and xenon [11]. During the study, the fission gas krypton was measured in-situ in a nuclear fuel for the first time and an investigation of the total fission gas content (Xe + Kr) of the HBS

* Corresponding author. Tel.: +49 7247951477; fax: +49 7247951590.
E-mail address: clive.walker@ec.europa.eu (C.T. Walker).

0022-3115/$ - see front matter © 2009 Elsevier B.V. All rights reserved.
doi:10.1016/j.jnucmat.2009.06.017

using depth profiling was performed. The results of this latter investigation confirmed that almost all of the gas lost from the fuel matrix is contained in the pores of the HBS and that the pores are overpressurised.

2. Fuel characteristics and irradiation history

The fuel section examined by SIMS was cut from the low power region of rod 12H3. Relevant fuel pellet and rod design characteristics are given in Table 1. The rod was of standard PWR design for Siemens' built reactors with a plenum above and below the fuel stack. The fuel rod cladding was a highly corrosion resistant zirconium alloy.

Rod 12H3 was irradiated in a Siemens built 15 × 15 fuel assembly in a commercial PWR reactor. Its irradiation spanned eight reactor cycles and lasted 2631 effective full power days. At the end of the fourth reactor cycle when the original fuel assembly had reached its nominal discharge burn-up of 60 MWd/kgHM the rod was transferred to a carrier assembly containing partially burnt fuel for further irradiation. The rod was subsequently introduced into a new carrier assembly at the beginning of each new reactor cycle. The fuel was discharged from the reactor in June 1997.

Table 2 shows the power history and burn-up evolution for rod 12H3. It is seen that during the first four cycles the average power rating fell from about 34–20 kWm^{-1}. After transfer to the carrier assembly the power rating decreased more gradually from 18 kW m^{-1} in the fifth cycle to 14 kW m^{-1} in the eighth and final cycle. The rod average burn-up at the end-of-life was 90 MWd/kgHM.

3. Fuel sample examined by SIMS

The plain of the cross-section surface analysed by SIMS was located approximately 31 cm from the bottom end of rod 12H3 and had a burn-up of about 65 MWd/kgHM. The burn-up was derived from the gross axial gamma scan for the rod (see Fig. 2, Ref. [11]), which was calibrated by chemical burn-up analysis of a fuel pellet extracted from the high power upper region of the fuel stack. The form of the gross axial gamma scan follows closely the axial burn-up distribution.

Table 1
Fuel pellet and rod design characteristics.

Pellet diameter (mm)	9.3
Initial enrichment (wt% ^{235}U)	3.5
Fuel density (%TD)	95
2D grain size[a] (m)	9–12
O/*M*	2.005
Diametrical gap (μm)	160–190
He fill gas pressure (bar)	22.5
Cladding material	Zr-based alloy

[a] Linear intercept.

Table 2
Power history and burn-up evolution in the high burn-up fuel rod.

Reactor cycle	Max. Av. linear power (kW m^{-1})	Cumulative Av. burn-up (MWd/kgHM)
1	34	19
2	29	37
3	23	48
4	20	59
5	18	67
6	17	72
7	16	82
8	14	90

The radial temperature distribution in the fuel during irradiation was calculated with the advanced version of the AREVA-NP fuel rod analysis and design code CARO-E [12]. This code takes into account the degradation of thermal conductivity of the fuel that occurs with increase in burn-up, both due to the build-up of fission products in the UO_2 lattice and the presence of gas filled pores in the high-burn-up structure. Apart from at the end of the first cycle when 1000 °C was reached, the fuel centre temperature at the axial location from which the SIMS sample was taken was between 500 and 600 °C throughout the irradiation.

4. Post-irradiation examination of rod 12H3 and the fuel-section analysed by SIMS

Numerous post-irradiation examinations have been performed on rod 12H3 and on the same fuel section on which the SIMS investigation was carried out. These include rod puncturing and mass spectrometry of the plenum gas, chemical burn-up analysis, optical microscopy, scanning electron microscopy (SEM) and EPMA. In addition, inductively coupled plasma mass spectrometry (ICP-MS) was carried out on fuel from the high burn-up sibling rod, 12C3. The results of some of these examinations have already been reported; e.g., SEM and EPMA [11], ICP-MS [13]. In this section, findings that have a relevance to the SIMS results and that were used as an aid to their interpretation are summarized.

4.1. Puncturing results

The fractional fission gas release determined by puncturing of rod 12H3 was 22% [11]. The isotopic composition of the Kr and Xe in the plenum is given in Table 3. The amounts of Xe and Kr

Table 3
Puncturing results for the isotopic composition of Kr and Xe in the plenum of rod 12H3.

Isotope	Abundance (at %)
^{83}Kr	5.1
^{84}Kr	40.3
^{85}Kr	5.1
^{86}Kr	49.4
^{131}Xe	3.8
^{132}Xe	26.8
^{134}Xe	27.8
^{136}Xe	41.7

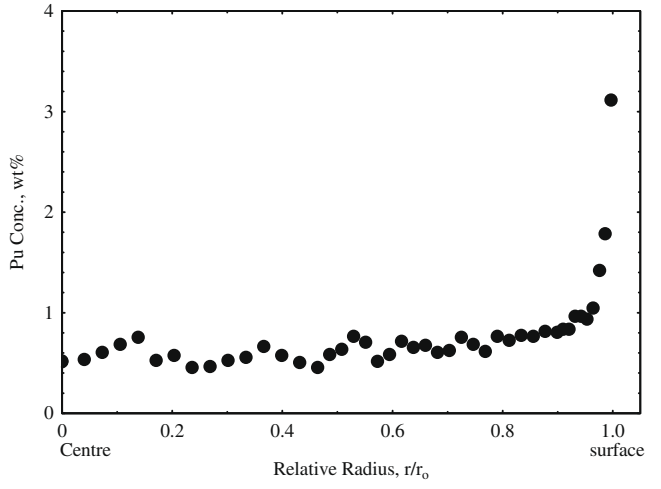

Fig. 1. EPMA results for the radial distribution of Pu in the cross-section of the fuel sample analysed by SIMS.

in the gas mixture corresponded to a Xe/Kr volume ratio of 10.8. This ratio is intermediate between the values for gas resulting from the fission of ^{235}U (Xe/Kr = 7) and the fission ^{239}Pu (Xe/Kr = 19) [14], confirming that Pu fission made an important contribution to the burn-up.

4.2. Optical microscopy

Optical microscopy was carried out on the fuel section used for the SIMS investigation. The microstructure of the fuel along a radius in the as-polished and etched state was examined at a magnification of 500×. Between the pellet centre and $r/r_o = 0.95$ the fuel exhibited the as-fabricated microstructure which consisted of equi-axed grains and large angular pores. The porosity varied between 3 and 5%. In the central region of the fuel isolated arrays of gas bubbles a few hundred nanometers in size were detected. This indicates that thermal diffusion of fission gas had occurred in the central region of the fuel at some point during the irradiation; most probably at the end of the first irradiation cycle, when the fuel centre temperature was around 1000 °C. A thin band of high burn-up structure was present at the pellet surface. In the region occupied by the high burn-up structure the porosity increased dramatically from around 5% at $r/r_o = 0.95$ to more than 10% at the fuel rim.

4.3. Electron probe microanalysis

EPMA was carried out on the same fuel section used for the SIMS investigation. The radial distributions of Pu, Nd, Cs and retained Xe were measured. In addition, EPMA electron absorption micrographs of the high burn-up structure were produced. Quantitative image analysis was subsequently carried out on these micrographs to determine the pore size distribution in the high burn-up structure.

4.3.1. Radial distribution of plutonium

The creation of Pu during the irradiation of UO_2 nuclear fuel is the result of capture by epithermal neutrons in the resonances of ^{238}U. The measured radial concentration profile for Pu is shown in Fig. 1. It is seen that Pu is uniformly distributed in the interior of the fuel, whereas its concentration increases steeply at the fuel rim due to enhanced neutron capture in this region. The concentration of Pu varies between 0.5 and 0.8 wt% in the fuel interior and increases to about 3.2 wt% over a distance of 250 μm at the fuel rim. The integral average concentration of Pu in the fuel cross-section was 0.8 wt%.

4.3.2. Radial distribution of neodymium

Neodymium is immobile in UO_2 nuclear fuel and therefore can be used as an indicator of the radial burn-up distribution and hence the local concentration of the fission products produced in the fuel lattice. The radial distribution of fission product Nd is shown in Fig. 2. It can be seen that in the interior of the fuel the Nd distribution is flat, whereas at the fuel rim it increases steeply due to the fission of Pu from neutron capture. The integral average concentration of Nd in the fuel cross-section was 0.63 wt%. The radial concentration profile for Nd indicates that in the interior of the fuel the burn-up was between 57 and 62 MWd/kgHM and reached about 140 MWd/kgHM at the pellet rim. These burn-ups were calculated using a total fission yield for Nd of 0.171 at% per 1 at% burn-up (0.097 wt% per 10 MWd/kgHM).

4.3.3. Radial distribution of caesium

The radial distribution profile for Cs is shown in Fig. 3. The form of profile is similar to that for Nd indicating that significant release of Cs from the fuel matrix had not occurred. The integral average concentration of Cs in the fuel cross-section was 0.52 wt%. This corresponds to a fission yield value of 0.15 at% per 1 at% burn-up which is within the expected range of 0.13–0.16 at% per 1 at% burn-up.

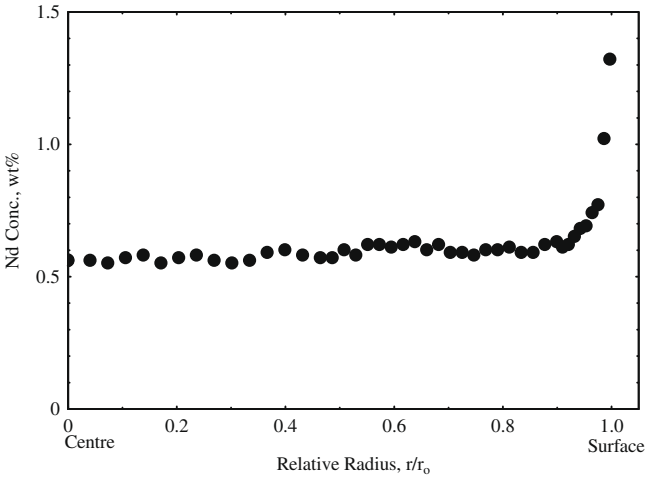

Fig. 2. EPMA results for the radial distribution of Nd in the cross-section of the fuel sample analysed by SIMS.

4.3.4. Radial distribution of xenon

The radial distribution of xenon is shown in Fig. 4. It is seen that Xe profile is flat in the central region of the fuel indicating that thermal release had not occurred. Moreover, the concentration of Xe in this region is about 0.85 wt% which corresponds to full retention. The measured concentration of Xe, however, drops sharply between $r/r_o = 0.95$ and fuel surface. This is due to the presence of the high burn-up structure.

4.3.5. Pore size distribution in the high burn-up structure

The spatial volume density and size distribution of the pores in the HBS at the rim of the fuel sample analysed by SIMS were measured using the AnalySIS® image processing software marketed by Olympus Soft Imaging Solutions GmbH, Germany. The measurements were performed on an EPMA electron absorption micrograph showing the microstructure in the vicinity of the fuel surface at a magnification of 500×. The micrograph was produced at an electron acceleration potential of 20 kV. Applying the

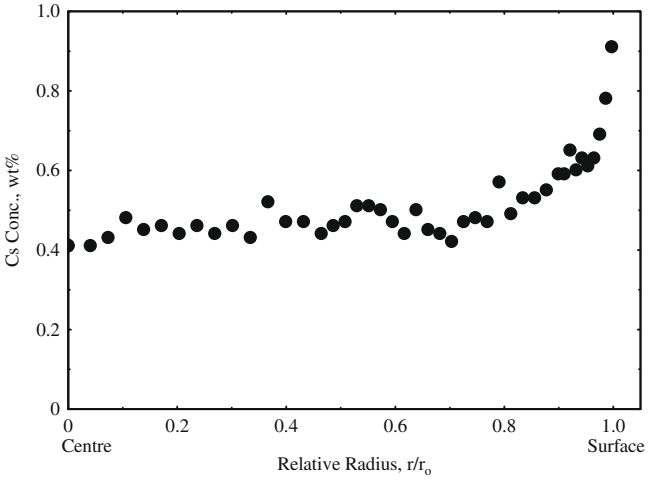

Fig. 3. EPMA results for the radial distribution of Cs in the cross-section of the fuel sample analysed by SIMS.

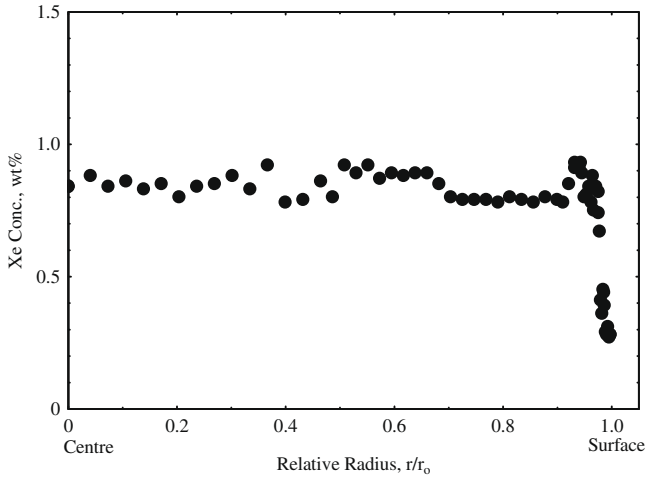

Fig. 4. EPMA results for the radial distribution of retained Xe in the cross-section of the fuel sample analysed by SIMS.

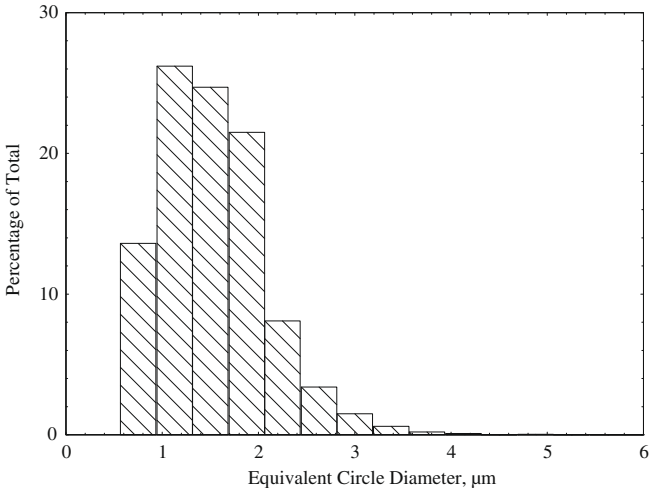

Fig. 6. Size distribution of the pores in the high burn-up structure at the surface of the fuel sample analysed by SIMS. The mean pore size is 1.52 ± 0.01 μm.

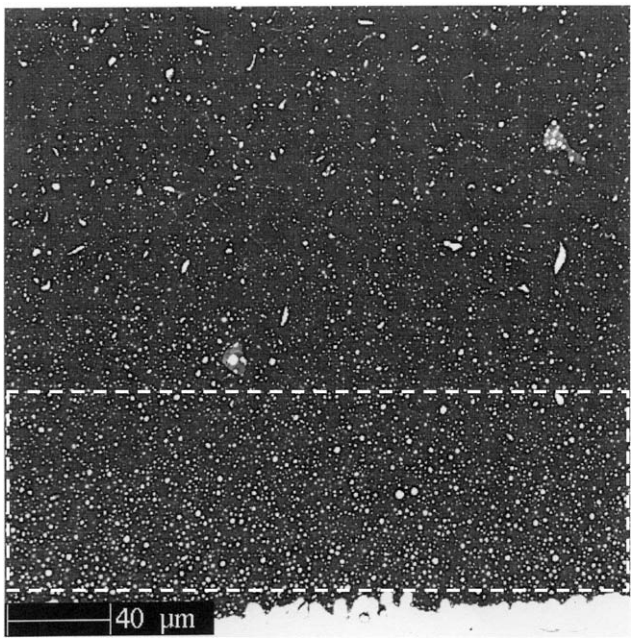

Fig. 5. EPMA electron absorption micrograph showing the microstructure at the surface of the fuel sample analysed by SIMS. The high concentration of micron size pores signifies the presence of the high burn-up structure. The pore size distribution and volume density were measured in the rectangular area delineated by the dashed lines.

equation of Kanaya and Okayama [15] the electron penetration in UO_2 at this energy was calculated to be 1.83 μm. The electron absorption micrograph is presented in Fig. 5. Pores appear as white spots in the micrograph and the high density of pores at the fuel rim signifies the presence of the HBS. The size distribution of the pores in the HBS at the fuel surface is shown in Fig. 6. The mean pore size derived from the data plotted in the histogram is 1.52 ± 0.01 μm. The volume pore density in the HBS was 8.8×10^7 pores per mm^3.

5. SIMS analysis

SIMS was carried using a CAMECA IMS-6F, double-focusing sector field instrument that had been specially shielded and modified for the analysis of irradiated nuclear fuel. A description of the installation can be found in Ref. [16]. A $(^{16}O)_2^+$ primary ion beam was general employed. The radial distributions of the isotopes of a single fission product or actinide element in the fuel matrix were measured simultaneously at the same location using identical instrument settings. The primary ion and secondary ion acceleration voltages were +15 and +5 kV, respectively, and beam currents of 50 nA (Cs), 150 nA (Kr, Xe, Nd, U and Pu) and 300 nA (Am and Cm) were employed. The mass resolution was normally about 1000, but for the analysis of the radial distributions of ^{243}Am, ^{244}Cm and ^{245}Cm a higher resolution of the order of 3000 was used. The ion intensity was measured along the fuel radius at intervals of 100 μm. This gave a radial ion intensity profile comprising about 32 data points. At each location the primary beam was scanned over an area measuring 100 × 100 μm in order to average out the effects of grain orientation and porosity on the generated ion intensity. Moreover, the secondary ion signal was collected in a 62 μm diameter diaphragm (field aperture 2) to avoid the collection of ions from the edges of the craters. The centre line of the first raster was located about 60 μm from the fuel rim and, at each radial position five adjacent intensity measurements were made 50 μm apart. The integration time for an individual isotope was either 0.5 or 1s and the total acquisition time at each radial position ranged from 367 (U and Pu) to 726 s (Cs).

Attention is drawn to the fact that the reported ion count rates and isotope ratios have not been corrected for mass interference by the isotope hydride or for mass basis effects [17].

It has been shown [18–20] that unlike solid substances, which are ionized at the fuel surface during sputtering, Xe and Kr leave the fuel as neutral atoms and they are ionized in the specimen chamber. Consequently, the ion signals for Xe and Kr are weak. The intensity of the ion signals were enhanced by using an oxygen leak ($P_{O_2} = 1.2 \times 10^{-6}$ mbar in the specimen chamber) and to separate the Xe and Kr signals from molecular interferences a 20 or 25 eV wide 50 eV centred energy gate was employed as recommended by Desgranges and Pasquet [18,19]. This energy gate was used for all the analyses reported in this article.

Depth profiles for ^{132}Xe and ^{84}Kr in the high burn-up structure at the fuel rim were produced using a focused beam 45 μm in diameter. Apart from this, the analysis conditions were the same as those used to measure the fission gas isotopes in the fuel matrix. In this analysis the variation in the ion intensity during sputtering was monitored for approximately 1 h (3639 s). Depth profiling was performed at seven locations about 150 μm apart beginning

at $r/r_o = 0.99$ and ending at $r/r_o = 0.81$. Accordingly, the first depth profile was situated about 45 μm from the fuel rim.

Ion maps showing the distributions of Kr, I, Te, Cs and Xe in the high burn-up structure were produced using a $(^{16}O)_2^+$ at a primary acceleration voltage of 15 kV. The $^{129}I^-$ and $^{130}Te^-$ ions were collected using a secondary acceleration voltage of −5 kV, all other ions were collected in the positive mode using a secondary acceleration voltage of +5 kV. The maps were constructed by superimposing between 150 and 200 raster scans of 5 to 50 s duration depending on the given isotope.

The distributions of ^{129}I and ^{130}Te were measured at the same location at the fuel surface using a beam current of 150 ρA and the same instrument settings. At 150 ρA the beam diameter is about 1.5 μm, which is similar to the size of the pores in the high burn-up structure. The distribution of ^{137}Cs was measured adjacent to the location where the distributions of ^{129}I and ^{130}Te were determined. A lower beam current of 50 ρA was employed, and consequently the $^{137}Cs^+$ ion map has a noticeably higher spatial resolution due to the smaller diameter of the primary ion beam.

The distributions of Xe and Kr in the high burn-up structure were investigated by measuring the distributions of ^{85}Rb and ^{133}Cs. These isotopes are the daughter products of ^{85}Kr (half-life, 10.75 years) and ^{133}Xe (half-life, 2.25 days) and since they are solids they are ionized in-situ in the fuel. For the purposes of this investigation a primary beam current of 200 ρA was employed.

For the measurement of the radial distributions of the fission products and actinide elements in the fuel matrix the current density of the primary ion beam was varied between 0.5 and 3.0 mA/cm^2 and for depth profiling in the high burn-up structure it was 9.4 A/cm^2. Measurements made with an interferometer microscope have shown that the sputtering rate of an unirradiated single crystal of UO_2 using a $(^{16}O)_2^+$ primary ion beam at an acceleration voltage of 12.5 kV is about 3.75×10^7 nm^3/nA/s [19]. Using this sputtering rate, the current densities quoted above and the total acquisition time it was calculated that a layer of material between 0.2 and 0.5 μm thick was sputtered from the sample surface during the analysis of the fission product and actinide elements in the fuel matrix and that the crater produced during depth profiling in the high burn-up structure was about 13 μm deep. Since, the sputtering rate will clearly be higher for polycrystalline irradiated nuclear fuel containing porosity than for an unirradiated UO_2 single crystal the above erosion depths are lower limits.

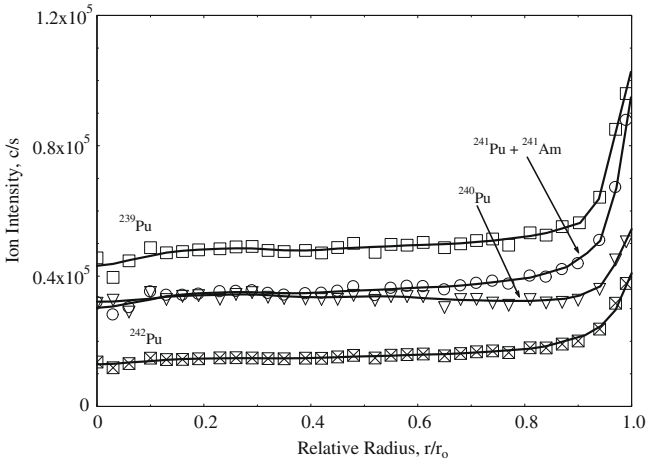

Fig. 7. Radial distribution of the major Pu isotopes in the fuel matrix. Isobaric interference exists between ^{241}Pu and ^{241}Am. The lines were computed by three point smoothing and serve to distinguish between the data for the different isotopes.

6. SIMS results

6.1. Radial distribution of plutonium and the minor actinides

The radial distributions of the major Pu isotopes in the fuel matrix are shown in Fig. 7. It can be seen that the Pu isotopes are uniformly distributed in the interior of the fuel, but increase in concentration sharply at the fuel surface. Fig. 8 shows the radial distribution of the minor actinide isotopes ^{243}Am, ^{244}Cm and ^{245}Cm. Since these minor actinide isotopes mainly result from neutron activation of plutonium their concentrations also increase dramatically at the fuel surface. As seen from the three plots the concentrations of the minor actinides are about 4× higher at the pellet rim than in the interior of the fuel. The radial distribution of ^{237}Np is shown in Fig. 9. The intensity profile is flat and does

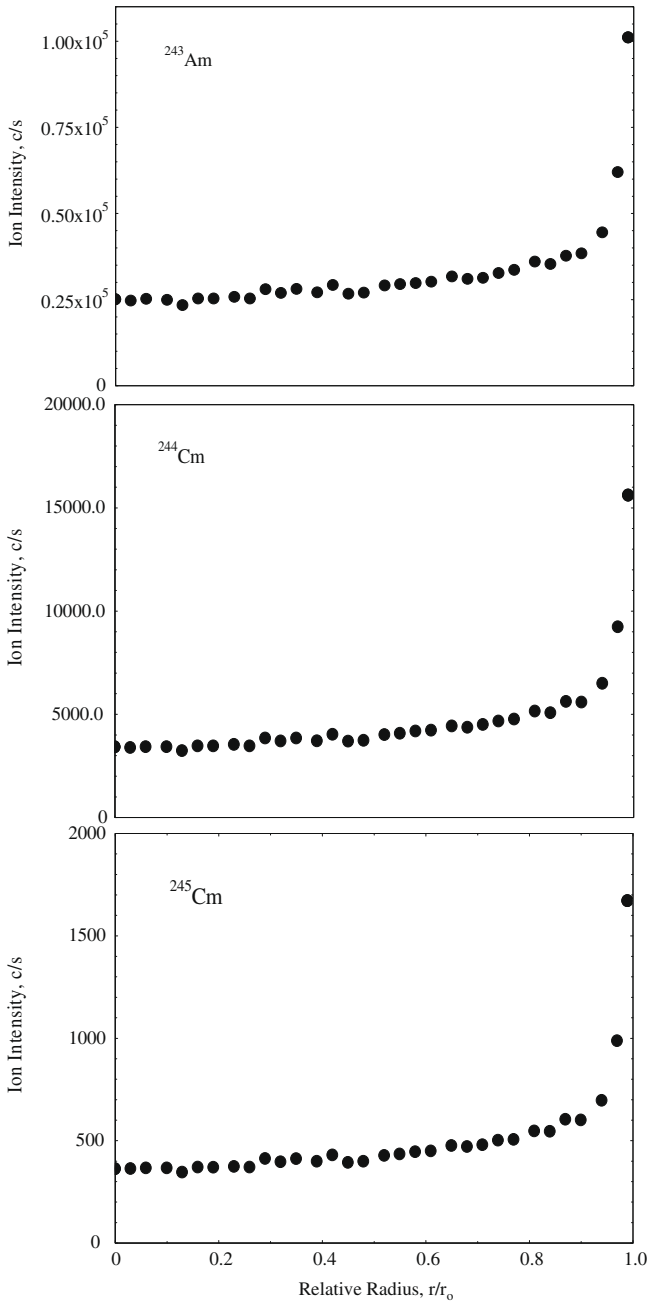

Fig. 8. Radial distributions of the minor actinide isotopes ^{243}Am, ^{244}Cm and ^{245}Cm in the fuel matrix.

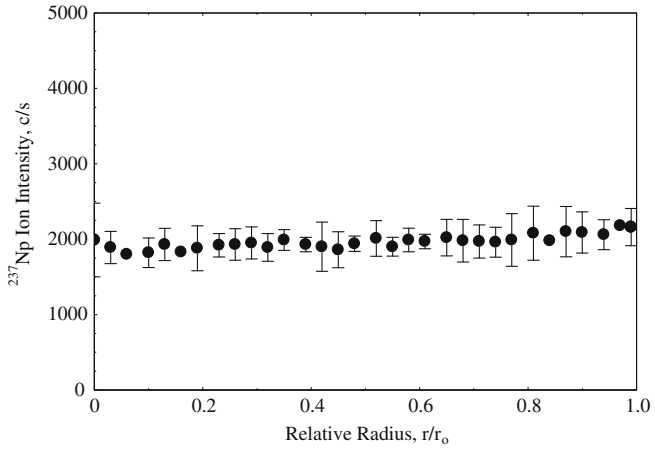

Fig. 9. Radial distribution of ^{237}Np in the fuel matrix. The error bars mark the confidence limits at the 95% level (2σ).

not exhibit an increase at the fuel surface like the other minor actinide isotopes measured.

6.2. Radial distribution of neodymium

The radial distributions of the stable Nd isotopes ^{144}Nd, ^{145}Nd, and ^{146}Nd, are shown in Fig. 10. As can be seen all three intensity profiles increase noticeably in the region between $r/r_o = 0.8$ and the fuel surface. The radial intensity profiles for stable isotopes ^{148}Nd and ^{150}Nd are not included in Fig. 10, because isobaric interference exists with ^{148}Sm and ^{150}Sm. The profiles, however, have the same form as the intensity profiles for ^{144}Nd, ^{145}Nd, and ^{146}Nd.

The average integrated ion intensity of the Nd isotopes determined from their measured radial profiles and the isotope abundance derived from the data is given in Table 4. The ion intensities for ^{148}Nd and ^{150}Nd were determined by multiplying the intensity measured at these masses by the weight fraction of Nd present derived from fission yield tables. The correction factor, which is burn-up dependent, was estimated to be 0.6 for mass 148 and 0.4 for mass 150. A correction for the difference in the ionisation yield of Sm and Nd was not applied. The data reported by Hervig et al. [21] reveal that the correction is <10% relative. Thus, it is small compared with that for the weight fractions of Nd and Sm at the masses 148 and 150.

Table 4
Average integral ion intensity of the Nd isotopes in the fuel cross-section measured by SIMS and the derived isotopic abundance.

Isotope	Ion intensity (c/s)	Isotope abundance (%)
^{144}Nd	4.09×10^5	42.5
^{145}Nd	1.37×10^5	14.2
^{146}Nd	2.00×10^5	20.8
^{148}Nd	1.08×10^5[a]	11.2
^{150}Nd	1.08×10^5[a]	11.3

[a] After correction for isobaric interference by samarium.

6.3. Radial distribution of caesium

The radial distributions of ^{133}Cs, ^{135}Cs and ^{137}Cs in the fuel matrix are shown in Fig. 11. The profiles are constructed from the average of two intensity measurements at each radial position. Again, the concentrations of all three isotopes increase markedly at the pellet surface. Further, it may be noticed that although about 25% of the ion signal at mass 137 emanates from ^{137}Ba, the distribution profiles for ^{137}Cs and ^{133}Cs are almost indistinguishable and show a slight decrease in the central region of the fuel.

6.4. Radial distributions of xenon and krypton

Fig. 12 shows the radial distributions of the stable Xe isotopes 131, 132, 134 and 136. It can be seen that whilst the profiles for ^{134}Xe and ^{136}Xe exhibit the usual pronounced increase at the fuel surface, the profiles for ^{131}Xe and ^{132}Xe do not. Attention is drawn to the fact that in the ^{132}Xe profile the data point closest to the fuel surface is lower than the rest. This point lies within the band of high burn-up structure at the fuel rim. Consequently, a drop in the ion intensity is exactly what would be expected, because where the high burn-up structure forms the fuel matrix is depleted in Xe (see Fig. 4).

The increase in the intensity at the fuel surface exhibited by ^{134}Xe and ^{136}Xe is assumed to be due to isobaric interference by the fission products Cs and Ba. Not only do these fission products increase in concentration at the fuel surface, but they also have much larger ion yields than Xe. Hence, their ion signals swamp the Xe ion signal. Consequently, of the four isotopes measured only

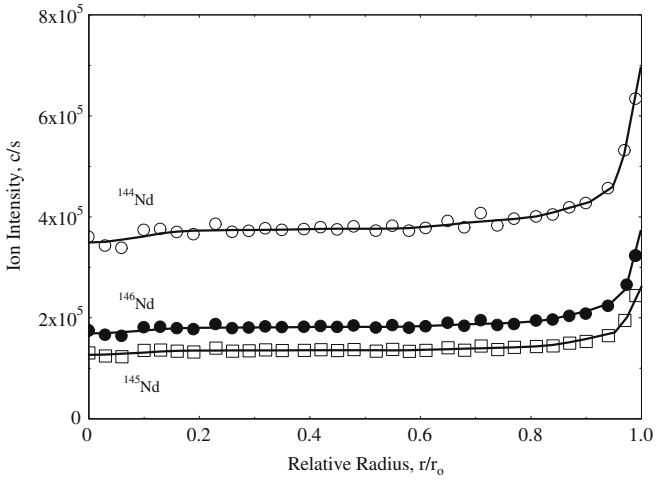

Fig. 10. Radial distributions of the stable Nd isotopes ^{144}Nd, ^{145}Nd and ^{146}Nd in the fuel matrix. The lines were computed by three point smoothing and serve to distinguish between the data for the different isotopes.

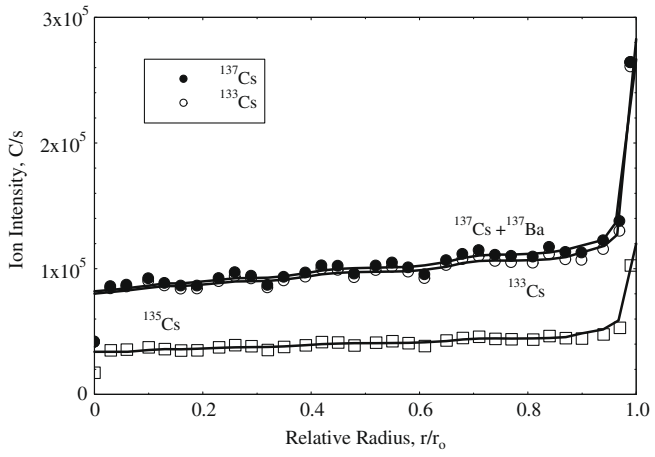

Fig. 11. Radial distribution of the Cs isotopes 133, 135 and 137 in the fuel matrix. Isobaric interference exists between ^{137}Cs and ^{137}Ba. The lines were computed by three point smoothing and serve to distinguish between the data for the different isotopes.

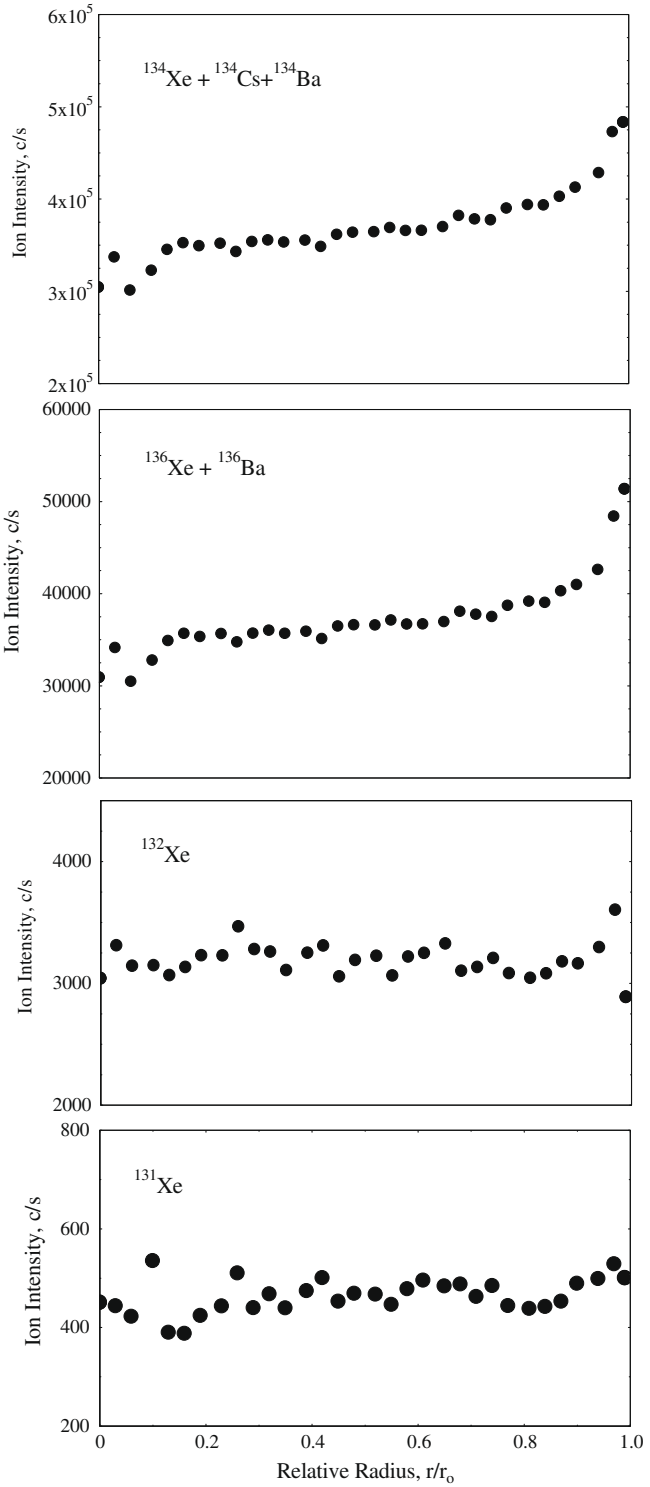

Fig. 12. Radial distributions of ^{131}Xe, ^{132}Xe, ^{134}Xe and ^{136}Xe in the fuel matrix. The ion intensity signal for the masses 134 and 136 increases at the fuel surface, whereas the signal for the masses 131 and 132 decreases.

^{131}Xe and ^{132}Xe can be utilised for the study of the behaviour of Xe by SIMS.

Fig. 13 shows the radial ion intensity profiles for ^{83}Kr, ^{84}Kr and ^{86}Kr, which are all stable isotopes. Only the ion intensity of ^{86}Kr decreases at $r/r_o = 0.99$ at the fuel rim where the high burn-up structure is present; the ion intensities of the other two isotopes ^{83}Kr and ^{84}Kr increase. For these latter two isotopes the observed increase in intensity at the fuel rim is assumed to be due to molecular interference by $^{82}SeH^+$ and $^{52}CrO_2^+$, respectively. The fission yield of ^{82}Se is similar to that of ^{83}Kr and H_2 is present in the Zircaloy cladding due to dissociation of the coolant water. Chromium is an alloying element of Zircaloy and diffuses into the fuel when the cladding contacts the fuel surface. The intensity of the $^{52}Cr^+$ ion signal was 3.5× higher at the fuel surface than at the pellet mid-radius. Isobaric interference exists between $^{86}Kr^+$ and $^{85}RbH^+$, but since ^{85}Rb is the daughter product of ^{85}Kr the radial distribution of this molecular ion follows that of $^{86}Kr^+$.

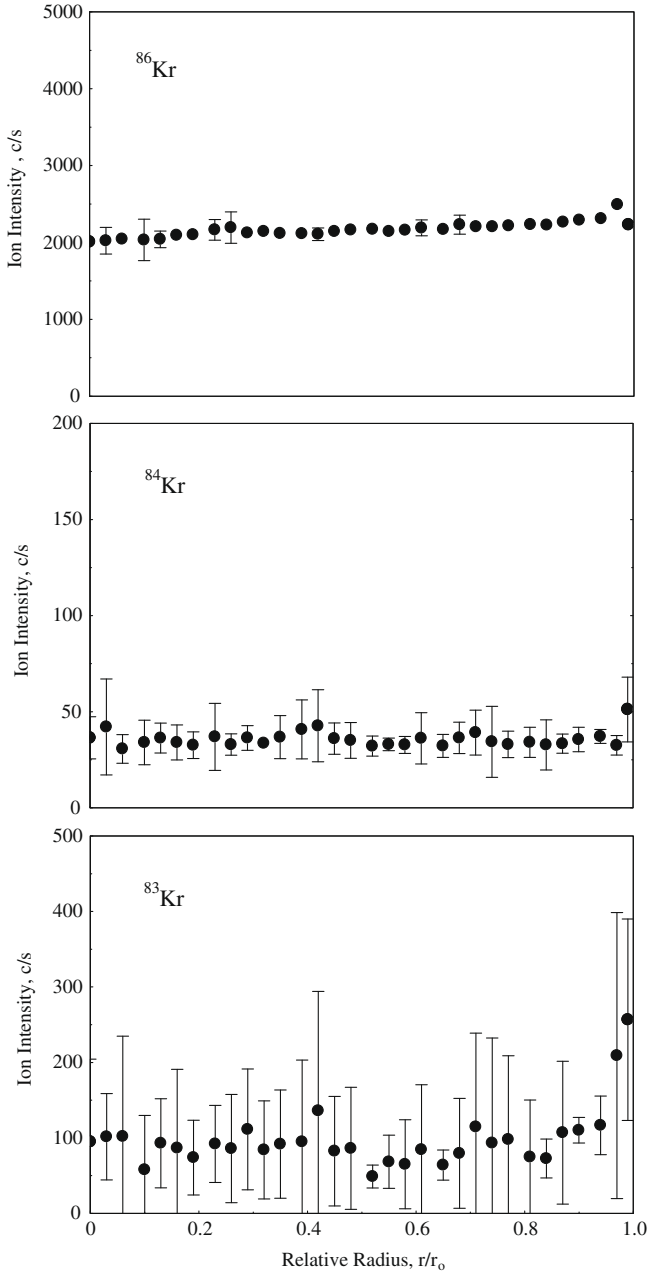

Fig. 13. Radial distributions of the stable Kr isotopes 83, 84 and 86 in the fuel matrix. The error bars mark the confidence limits at the 95% level (2σ).

6.5. Behaviour of xenon and krypton in the high burn-up structure

Examples of depth profiles for ^{132}Xe and ^{84}Kr in the high burn-up structure are shown in Fig. 14. The intensity spikes in both traces correspond to the gas released from the pores in the struc-

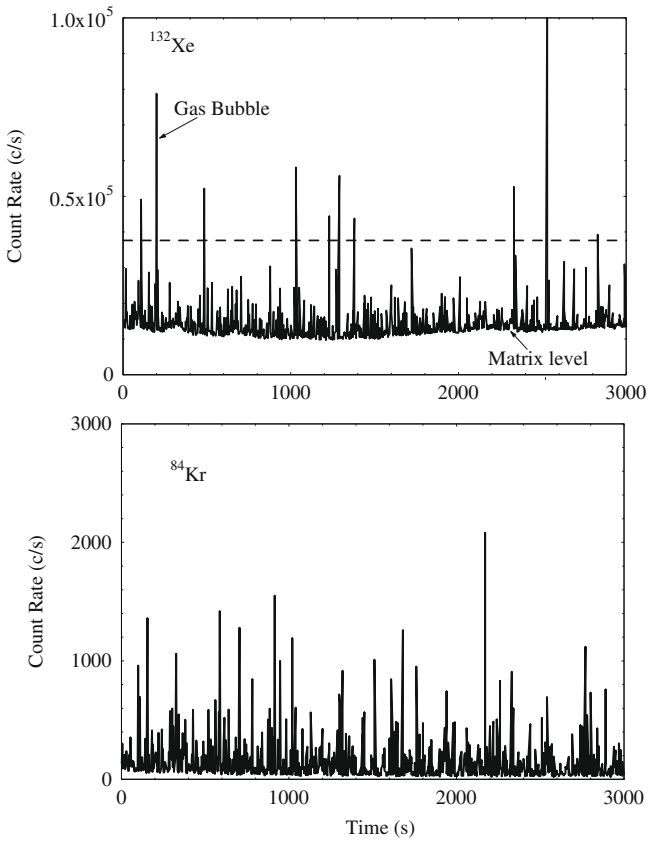

Fig. 14. Depth profiles for ^{132}Xe and ^{84}Kr in the high burn-up structure. The intensity spikes mark the location of gas pores in the microstructure. The dashed line on the Xe depth profile indicates the ion intensity that is equal to a gas pressure of 25 MPa in the pores. Time corresponds to erosion depth.

ture during sputtering. Each spike is the result of the expulsion of gas from the pore population in the sputtered layer. Attention is drawn to the fact that in the case of the high burn-up structure the spikes are not the result of gas release from a single pore. It will be noted that few of the intensity spikes on the Xe and Kr traces in Fig. 14 coincide. This is because in SIMS the isotopes are measured consecutively by mass switching. (In the present case, the Xe and Kr isotopes were measured at intervals of about 2 s.)

The radial variation of the ^{132}Xe ion intensity signal from depth profiling at radial intervals in the outer region of the fuel is shown in Fig. 15. The profile represents the radial distribution of the total amount of ^{132}Xe retained in the fuel in the UO_2 lattice, on grain boundaries, and in pores and gas bubbles. It can be seen that in the radial interval between $r/r_o = 0.95$ and the fuel surface where the high burn-up structure is present the ^{132}Xe ion intensity increases sharply and is about three times higher at the fuel rim than at $r/r_o = 0.90$.

Ion maps for the distribution of the stable fission product isotopes ^{133}Cs and ^{85}Rb in the high burn-up structure are presented in Fig. 16. These isotopes are the decay products of ^{133}Xe and ^{85}Kr, and since they are solids they will be ionized in the conventional manner during the sputter process. It is clear from the maps that the fission gases Xe and Kr were present together in the pores of the high burn-up structure. Pores that unambiguously show evidence of having contained ^{133}Xe and ^{85}Kr are circled.

It is highly improbable that the Cs and Rb detected in the pores have migrated there from the fuel matrix. At the temperature prevailing close to the fuel surface, ~500 °C, athermal diffusion predominates, which proceeds extremely slowly [22]. Accordingly, in the literature it is well documented that Cs is immobile in the

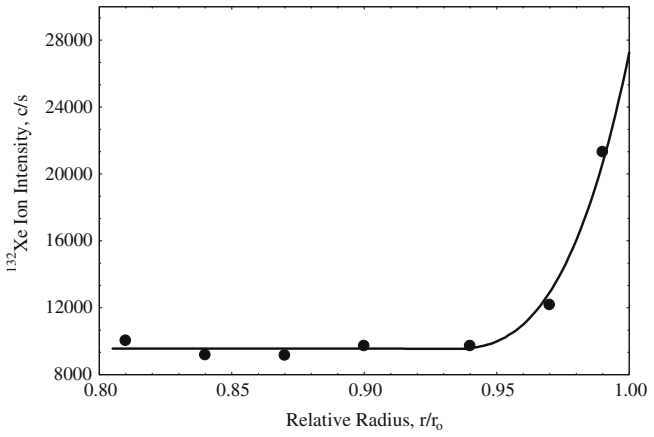

Fig. 15. Depth profiling results for the radial distribution of ^{132}Xe retained in the fuel matrix in the UO_2 lattice, on grain boundaries and in gas pores and bubbles in the outer region of the fuel between $r/r_o = 0.8$ and the fuel surface.

outer region of UO_2 fuel, and that, in contrast to the fission gases it concentration in the fuel matrix is unaffected by the formation of the high burn-up structure (see e.g., Ref. [23]). Rubidium, like Cs, is an alkali metal earth of group 1A of the Periodic Table and hence will behave similar to Cs. Moreover, fission fragments (fission products that possess all or part of the kinetic energy received from the fission event) that interact with gas bubbles or pores course resolution of the atoms that they contain rather than implant matter into them (see e.g., Refs. [24,25]).

6.6. Behaviour of the volatile fission products iodine, tellurium and caesium in the high burn-up structure

Ion maps showing the distribution of ^{129}I, ^{130}Te and ^{137}Cs in the high burn-up structure at the fuel rim are contained in Fig. 17. From the maps it appears that the three fission products behave differently. Caesium is clearly present in most of the pores of the high burn-up structure, whereas Te seems to have concentrated in certain pores only. Iodine, on the other hand, is relatively uniformly distributed which may indicate that it is also on the UO_2 grain boundaries as well as in the pores. The area of high iodine concentration in the ^{129}I ion map might point to the presence of a fission product iodide (e.g., TeI_2, CsI_2) as it is appears too large to be a gas pore.

7. Discussion

7.1. Behaviour of plutonium and the minor actinides

The concentrations of all the actinide isotopes analysed except ^{237}Np show a sharp increase at the fuel pellet surface. ^{237}Np behaves differently because it is produced by the capture of thermal neutrons by ^{235}U, whereas all the Pu, Am and Cm isotopes originate from the capture of epithermal neutrons by ^{238}U. The capture of thermal neutrons by ^{235}U is only weakly dependent on radial position (reflecting the thermal flux depression), whereas the capture of epithermal neutrons by ^{238}U is concentrated in the outer region of the fuel. Consequently, ^{237}Np is relatively uniformly dispersed in the fuel, whereas the concentrations of the Pu, Cm and Am isotopes increase steeply in the vicinity of the fuel surface. ^{237}Np is also a decay product of ^{241}Am and about 15% of the Np present was formed by this route. In a similar SIMS study carried out concurrently with this one by Desgranges et al. [26] the radial distribution of ^{237}Np was also found to differ from that of the other actinide isotopes measured.

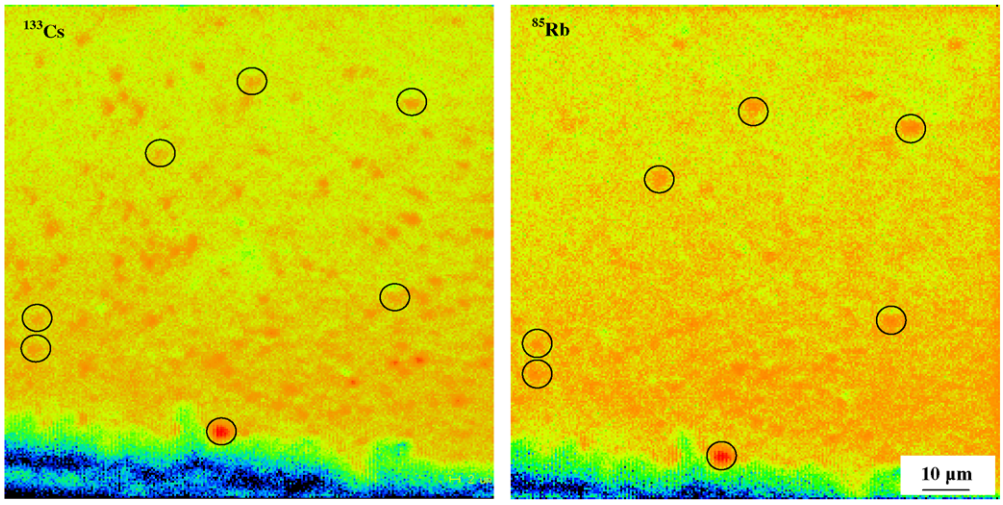

Fig. 16. Gas bubbles in the high burn-up structure as revealed by ion maps for ^{133}Cs and ^{85}Rb, the decay products of ^{133}Xe and ^{85}Kr. The fission gases Xe and Kr are together in the bubbles. The colour coding correlates with the local ion intensity. Black is low; red is high.

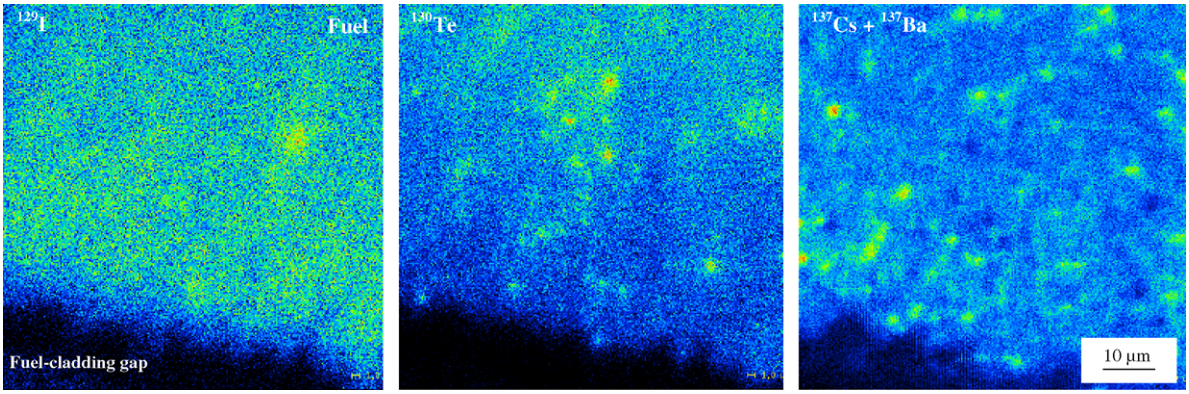

Fig. 17. Ion maps showing the distributions of ^{129}I, ^{130}Te and ^{137}Cs (^{137}Ba) in the high burn-up structure at the fuel rim.

The isotopic composition of plutonium obtained from the radial distribution of the isotopes measured by SIMS (Fig. 7) is given in Table 5. This Table gives the average isotopic composition of Pu in the fuel cross-section and the isotopic composition of Pu in the central region of the fuel and at the fuel periphery. The abundance of ^{241}Pu (8.7%) was derived by correcting the chemical burn-up analysis result in Table 5 for radioactive decay during 10 years. The abundances of the other isotopes were obtained by normalising the measured data to 91.3%. It is evident from Table 5 that the isotopic composition of Pu produced at the fuel periphery is slightly different from that produced in the central region of the fuel. That formed at the fuel periphery contains more ^{239}Pu and ^{242}Pu, and less ^{240}Pu. These differences may be explained by differences in the energy spectrum of the neutron flux at the two locations.

Table 5
Isotopic composition of Pu from the radial distribution of the isotopes measured by SIMS.

Pu isotope	Abundance (%)		
	Cross-section average (65 MWd/kgHM)	r/r_o = 0.2 (58 MWd/kgHM)	r/r_o = 0.97 (78 MWd/kgHM)
^{239}Pu	46.2	45.2	48.7
^{240}Pu	29.4	32.2	25.5
^{241}Pu	8.7[a]	8.7[a]	8.7[a]
^{242}Pu	15.7	13.8	17.1

[a] Theoretical abundance derived from the chemical burn-up analysis result after applying a correction for radioactive decay during 10 years.

To confirm their correctness, the SIMS profiles for the actinide isotopes were compared with the isotope distributions calculated with the new version of the TUBRNP burn-up model of the TRANSURANUS code [27] and the Monte-Carlo burn-up code ALEPH [28]. The current versions of the TUBRNP model and the ALEPH code have the capability to calculate the shape of the radial isotope profile, but they cannot compute the concentration level of the isotope. The measured and calculated radial distribution of the actinide isotopes were similar in all cases. The good agreement obtained is exemplified in Fig. 18 by the results for ^{240}Pu, ^{237}Np and ^{244}Cm.

7.2. Behaviour of neodymium and determination of the radial burn-up profile

The concentration of all the Nd isotopes analysed increased at the fuel surface as a result of an increase in the local burn-up caused by the fission of Pu resulting from neutron capture by ^{238}U.

Since neodymium is immobile in nuclear fuel its local concentration can be used as an indicator of the local burn-up. The radial burn-up distribution in the fuel sample investigated by SIMS had

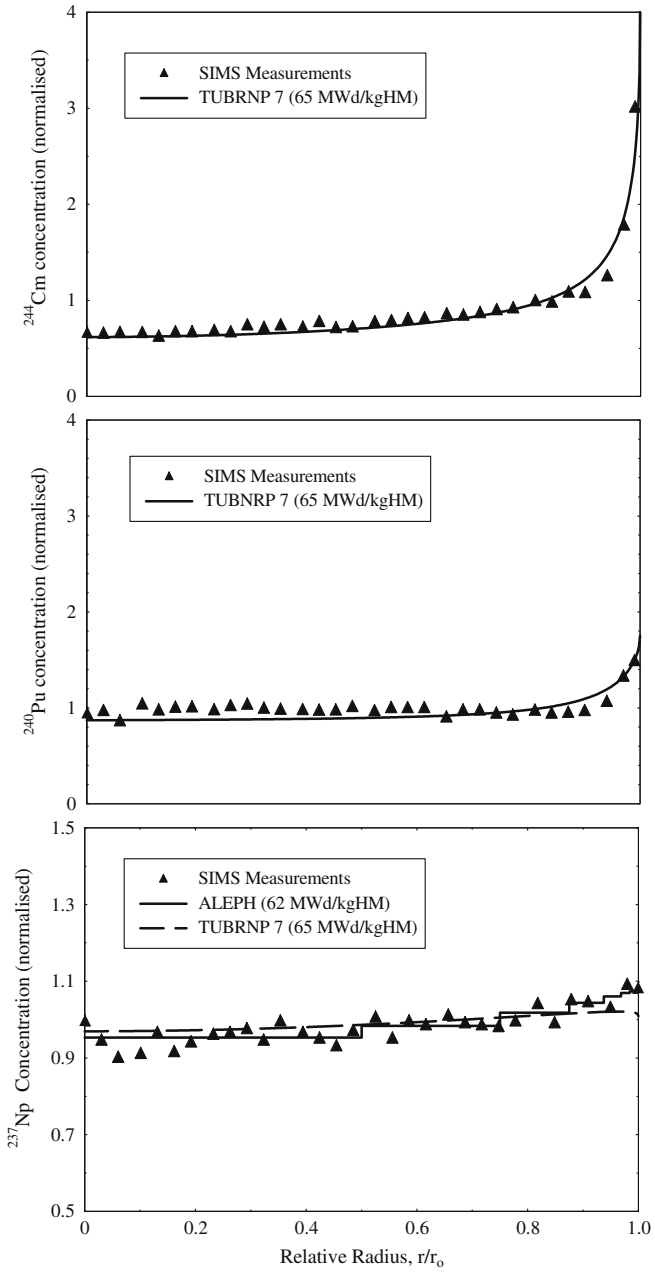

Fig. 18. Comparison of the radial profiles for ^{237}Np, ^{240}Pu and ^{242}Cm measured by SIMS with the radial isotope distributions calculated by the TUBRNP model [27] and the ALEPH burn-up code [28].

been earlier determined from the radial distribution of Nd measured by EPMA (see Section 4.3 and Fig. 2). The average integral concentration of Nd in the fuel cross-section was found to be 0.63 wt%. Since the average burn-up of the SIMS sample was 65 MWd/kgHM (determined from the gross gamma scan after calibration by chemical burn-up analysis [11]) it follows that 0.097 wt% Nd equals 10 MWd/kgHM. Using this relationship, it can be shown from the radial Nd profile in Fig. 2 that the burn-up over the fuel cross-section varied from about 60 MWd/kgHM in the interior of the fuel to 140 MWd/kgHM at the fuel periphery.

Valot et al. [29] have demonstrated that the radial burn-up profile in nuclear fuel can be determined from the radial distribution of the Nd isotopes measured by SIMS. They used the isotopic ratio $\frac{^{145}Nd+^{146}Nd}{^{238}U}$, which was calibrated against burn-up using a fuel sample whose burn-up had been determined by isotopic dilution analysis. The authors state that the error on the burn-up value obtained by this method is ±5 MWd/kgHM. However, the fission yields of the Nd isotopes change during irradiation, because, for instance, the relative contributions of the main fissile isotopes ^{235}U and ^{239}Pu changes considerably with burn-up. Consequently, the enrichment and burn-up of the reference fuel must be similar to that of the fuel sample whose burn-up is to be determined. A suitable reference fuel may not always be available. Therefore, in the present work the average burn-up of the fuel sample, *Bu*, was calculated from the SIMS results for the isotopic abundances of ^{145}Nd, ^{146}Nd and ^{148}Nd and the EPMA data for the elemental concentration of Nd in Fig. 2 using the following equation.

$$Bu = \frac{9.380 \cdot C_{Nd} \cdot a_i}{(\frac{m_i}{m_{UO_2}}) \cdot FY} \text{ MWd/kgHM} \quad (1)$$

where C_{Nd} is the integral average concentration of Nd in the fuel cross-section measured by EPMA (0.63 wt%), 9.380 is the factor for converting the burn-up units from at% to MWd/kgHM (assuming a fission energy of 200 MeV), a_i is the isotope abundance measured by SIMS, m_i is the mass of the Nd isotope, m_{UO_2} is the atomic mass of UO_2 and FY is the fission yield. The fission yield values used are composed of the fission yields for ^{235}U and ^{239}Pu obtained from the compilation of Meek and Rider [30]. From the composition of the puncture gas it is assumed that 70% of fissions occurred in ^{235}U and 30% in ^{239}Pu (see Subsection 4.1.).

The average burn-up determined from the abundance of ^{148}Nd was 72 MWd/kgHM, whereas using the combined abundances of ^{145}Nd and ^{146}Nd a burn-up of 59 MWd/kgHM was obtained. The burn-up of 65 MWd/kgHM determined by EPMA (see Section 4) lies in between these two values. Using ^{148}Nd has the advantage that the fission yields are similar for ^{235}U and ^{239}Pu (0.0169 and 0.0166, respectively). However, a correction has to be applied for isobaric interference by ^{148}Sm and the magnitude of this at high burn-up is uncertain. The isotopes ^{145}Nd and ^{146}Nd, on the other hand, are affected by neutron capture by ^{145}Nd during irradiation and hence their concentrations in the fuel are different from the values calculated from the fission yield. Therefore, the sum of the abundances of the two isotopes was used to calculate the burn-up. This also has the advantage that the fission yield (0.0649) is about four times higher and the isotope abundance (0.3499) is about three times higher than the values for ^{148}Nd (0.0168 and 0.1124, respectively).

Knowing the average cross-section burn-up of the sample, the radial burn-up profile in the fuel can be determined from the measured radial distribution of the Nd isotope. The radial profiles for ^{145}Nd and ^{146}Nd in Fig. 10 indicate that the burn-up increased by a factor of two at the fuel surface from about 55 to 112 MWd/kgHM. Thus, the increase in burn-up at the fuel surface measured by SIMS is somewhat lower than that measured by EPMA (see Subsection 4.3). The disparity can be explained by the fact that the ion signal was collected from an area measuring 100 × 100 μm, whereas the X-ray signal in EPMA was collected from a spot about 0.8 μm in diameter. Since the burn-up increases steeply in the vicinity of the fuel rim these differences in the size of the region of excitation clearly dictate the magnitude of the burn-up value measured.

7.3. Behaviour of the fission gases Xe and Kr in the high burn-up structure

It is evident from the SIMS depth profiles in Fig. 14 and in the ion maps in Fig. 16 that the pores in the high burn-up structure contain Xe and Kr. In Fig. 19 the ^{132}Xe profile measured in the outer region of the fuel by depth profiling at high current density

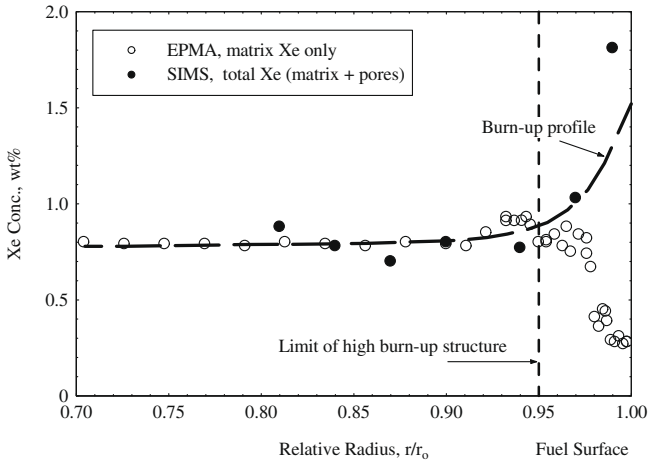

Fig. 19. The local concentration of retained Xe in the outer region of the fuel as measured by SIMS and EPMA. The burn-up profile determined from the local concentration of Nd measured by EPMA is included for the purposes of comparison.

(Fig. 15) is superimposed on the EPMA concentration profile for the radial distribution of Xe retained in the fuel matrix (Fig. 4). Also included in the plot for the purposes of comparison is the burn-up profile determined from the local concentration of Nd measured by EPMA (Fig. 2). It can be seen from Fig. 19 that in the radial interval between $r/r_o = 0.95$ and the fuel surface, where the HBS is present, SIMS measures a steep increase in the concentration of Xe as it detects the gas in the pores. The fact that the increase in gas concentration measured at the fuel rim by SIMS is greater than the increase in the local burn-up suggests that almost all the gas missing from the UO_2 matrix is contained in the pores of the high burn-up structure.

During depth profiling the Xe count rate obtained from the high burn-up structure during SIMS depth profiling varied between 11,760 and 123,000 c/s. The former count rate clearly corresponds to the concentration Xe in the grains of the high burn-up structure, which from EPMA is about 0.25 wt%, whereas the higher count rates recorded are the results of ion contributions from the gas contained in the pores of the high burn-up structure. Assuming that the ion yield of Xe in the pores is the same as that of Xe in the fuel matrix then the highest ion count rate measured (123,000 c/s) corresponds to a Xe concentration of 2.6 wt%. From the variation in the magnitude of the intensity spikes in the Xe depth profile in Fig. 14 it is evident that Xe content in the sputtered layers varied between the two extremes of 0.25 and 2.6 wt%.

During the sputtering time of 3000 s a total of 4.29×10^7 counts for Xe were accumulated. Of this number, 9.26×10^6 counts originated from Xe retained in the fuel matrix. The remaining counts resulted from Xe in the pores of the high burn-up structure. Taking the matrix counts (9.26×10^7) to be equivalent to a concentration of 0.25 wt%, the total number of Xe counts measured corresponds to a concentration of 1.16 wt%. The concentration of Xe created at $r/r_o = 0.98$ were the depth profile was made is calculated to be 1.14 wt%. Thus, the total amount of Xe detected in the high burn-up structure by SIMS depth profiling is in good agreement with the amount created. From this finding it is deduced that little if any gas was released from the high burn-up structure during the irradiation.

An important question with implications for the behaviour of the high burn-up structure during a RIA or a loss of coolant accident (LOCA) is the pressure of the gas in the pores of the high burn-up structure. For the low power sample from 12H3 the maximum gas pressure in the pores of the high burn-up structure is calculated from Eq. (2) to be 230 MPa, which corresponds to the maximum pressure that is sustainable by the fuel [1]. There are, however, only 11 points in the Xe depth profile in Fig. 14 where the measured ion intensity gives a Xe concentration that corresponds to a gas pressure that is in excess of 25 MPa according to Eq. (2). Although relatively low, the latter pressure is about 10× higher than the average surface tension pressure of the pores ($2\gamma/r$) which is 2.6 MPa, assuming $\gamma = 1$ Jm^{-2} and the average pore radius to be 0.76 μm (Fig. 6). From the average integral concentration of gas in the pores in the volume of material sputtered during depth profiling, 0.91 wt%, the average pressure of the gas in the pores is about 45 MPa. Thus, the pores of the high burn-up structure are overpressurised, but generally not excessively so.

It is well known that at high pressure and temperature, gas deviates from the perfect gas law. To account for any deviation, the pressure of gas in the pores of the high burn-up structure was calculated using the hard sphere equation of state of Brearly and MacInnes [31] which is written:

$$P = \left(\frac{nkT}{V}\right)(1 + y + y^2 + y^3)(1 - y)^{-3} \quad (2)$$

where n is the number of moles of gas (Xe + Kr) in the pores, k is the Universal Gas Constant expressed in atm/cm^3, y is the reduced density, T is the local fuel temperature and V is the volume fraction of the pores. The reduced density, y, is given by $\left(\frac{\pi d^3}{6}\right)\left(\frac{N_g}{V}\right)$, where d is the diameter of a Xe atom, which is taken to be 0.39 nm (see Fig. 1, ref. [31]) and N_g is the number of gas atoms in the pores. The local fuel temperature, T, was taken to be 400 °C and the volume fraction of the pores, V, was taken to be 0.162. The latter value was obtained from the EPMA electron absorption micrograph in Fig. 5.

8. Conclusions

For the study of the in-pile behaviour of fission products and actinides in nuclear fuel SIMS is a powerful complimentary analytical tool to EPMA. Its principal advantage lies in its low limit of detection; about 0.001 ppm compared with 200 ppm for EPMA. This enables the analysis of fission products of low fission yield, such as I, Rb and Br, which are implicated in stress corrosion cracking of Zircaloy cladding, as well as the investigation of the minor actinides, Np, Am and Cm. Further advantages include the capability to detect the fission gas Kr and to detect the fission gas contained in gas pores and bubbles in the fuel independent of their size.

The main disadvantage of SIMS, if the problem of quantification is neglected, is that mass interference is wide spread in the secondary ion spectra obtained from irradiated nuclear fuel. For example, of the five stable Nd isotopes 144, 145, 146, 148 and 150, only 144, 145 and 146 are interference free. Moreover, owing to mass interference, ^{131}Xe and ^{132}Xe and ^{86}Kr are the only isotopes that can be used to measure the radial distribution of the fission gases.

From the different SIMS investigations reported in this article and the considerations in the previous section a number of conclusions can be drawn.

- The radial distribution of Np in irradiated UO_2 fuel differs from that of Pu and the other minor actinides Am and Cm. This is because ^{237}Np is produced by the capture of thermal neutrons by ^{235}U, whereas the Pu, Am and Cm isotopes originate from the capture of epithermal neutrons by ^{238}U.
- Using a suitable calibration method, the average cross-section burn-up and the burn-up distribution along the pellet radius can be obtained from SIMS analysis of the radial distribution of one or more of the stable Nd isotopes. From the radial distributions of ^{145}Nd, ^{146}Nd and ^{148}Nd it was calculated that the

average burn-up of the fuel sample was in the range 59 to 72 MWd/kgHM , and that the burn-up increased by a factor of two at the fuel surface.

- The fission gas Kr behaves similar to Xe. In the high burn-up structure the two fission gases are together in the pores. By combining SIMS and EPMA results for the radial distribution of Xe in the outer region of the fuel and using depth profiling to determine the relative proportions of gas in the pores and the fuel matrix it was finally confirmed that almost all of the gas missing from the fuel matrix is contained in the pores of the high burn-up structure. The pressure of the gas in these pores was derived from SIMS depth profiling results for Xe and Kr in the high burn-up structure. The pores are overpressurised, but generally not excessively so. In fact, few of the pores present are sufficiently overpressurised to initiate energetic fragmentation of the fuel during a RIA or LOCA.
- In addition to the fission gases Xe and Kr, the pores of the high burn-up structure contain the volatile fission products Te, Cs, I and Rb (and almost certainly Br). Thus, the partial pressures of these fission products need to be taken into account when calculating the level of pressure in the pores.

References

[1] C.T. Walker, P. Knappik, M. Mogensen, J. Nucl. Mater. 160 (1988) 10.
[2] K. Lassmann, C. O'Carroll, J. van de Laar, C.T. Walker, J. Nucl. Mater. 208 (1994) 223.
[3] K. Lassmann, C.T. Walker, J. van de Laar, F. Lindström, J. Nucl. Mater. 226 (1995) 1.
[4] C.T. Walker, J. Nucl. Mater. 275 (1999) 56.
[5] C.T. Walker, T. Kameyama, S. Kitajima, M. Kinoshita, J. Nucl. Mater. 188 (1992) 73.
[6] C.T. Walker, J. Anal. At. Spectrom. 14 (1999) 447.
[7] C.T. Walker, J. Phys. D: Appl. Phys. 13 (1980) 2175.
[8] M. Verwerft, J. Nucl. Mater. 282 (2000) 97.
[9] M. Mogensen, J.H. Pearce, C.T. Walker, J. Nucl. Mater. 264 (1999) 99.
[10] T. Fuketa, H. Sasajima, Y. Mori, K. Ishijima, J. Nucl. Mater. 248 (1997) 249.
[11] R. Manzel, C.T. Walker, J. Nucl. Mater. 301 (2002) 170.
[12] F. Sontheimer, H. Landskorn, IAEA Tech. Committee Mtg. on Nuclear Fuel Behaviour at High Burn-up and its Experimental Support, Windermere, UK June 2000, Report IAEA-TECDOC-1233, 2001, p. 105.
[13] C.T. Walker, V.V. Rondinella, D. Papaioannou, S. Van Winckel, W. Goll, R. Manzel, J. Nucl. Mater. 345 (2005) 192.
[14] R.J. White, S.B. Fischer, P.M.A. Cook, R. Stratton, C.T. Walker, J. Nucl. Mater. 288 (2001) 43.
[15] K. Kanaya, S.O. Kayama, J. Phys. D: Appl. Phys. 5 (1972) 43.
[16] S. Brémier, R. Hasnaoui, S. Portier, O. Bildstein, C.T. Walker, Microchim. Acta 155 (2006) 113.
[17] Y. Ranebo, M. Eriksson, G. Tamborini, N. Niagolova, O. Bildstein, M. Betti, Microsc. Microanal. 13 (2007) 179.
[18] L. Desgranges, B. Pasquet, Nucl. Instrum. Methods B215 (2004) 545.
[19] L. Desgranges, Ch. Valot, B. Pasquet, J. Lamontagne, T. Blay, I. Roure, Nucl. Instrum. Methods B266 (2008) 147.
[20] S. Portier, S. Brémier, R. Hasnaoui, O. Bildstein, C.T. Walker, Appl. Surf. Sci. 225 (2008) 1323.
[21] R.L. Hervig, F.K. Mazdab, P. Williams, Y. Guan, G.R. Huss, L.A. Leshin, Chem. Geol. 227 (2006) 83.
[22] S. Brémier, C.T. Walker, Radiat. Eff. Defects Solids 157 (2002) 311.
[23] C.T. Walker, C. Bagger, M. Mogensen, J. Nucl. Mater. 240 (1996) 32.
[24] J.A. Turnbull, J. Nucl. Mater. 38 (1971) 203.
[25] R.S. Nelson, J. Nucl. Mater. 25 (1968) 227.
[26] L. Desgranges, B. Pasquet, Ch. Valot, I. Roure, J. Nucl. Mater. 385 (2009) 99.
[27] A. Schubert, P. Van Uffelen, J. van de Laar, C.T. Walker, W. Heck, J. Nucl. Mater. 376 (2008) 1.
[28] W. Haeck, B. Verbooman, Nucl. Sci. Eng. 156 (2007) 180.
[29] C. Valot, L. Desgranges, B. Pasquet, J. Lamontagne, J. Noroit, T. Blay, I. Roure, in: Proceedings of European Working Group on Hot Laboratories and Remote Handling, Petten, The Netherlands, May 2005.
[30] M.E. Meek, B.F. Rider, Compilation of Fission Product Yields, Vellicitos Nuclear Centre, General Electric, Report NEDO-12154-1, 1974.
[31] I.R. Brearly, D.A. MacInnes, J. Nucl. Mater. 95 (1980) 389.